Cellular/Molecular

Integrin β1 Signals through Arg to Regulate Postnatal Dendritic Arborization, Synapse Density, and Behavior

M. Sloan Warren,[1,2]* William D. Bradley,[2]* Shannon L. Gourley,[2,5] Yu-Chih Lin,[2] Mark A. Simpson,[2] Louis F. Reichardt,[6] Charles A. Greer,[1,3,4] Jane R. Taylor,[1,5] and Anthony J. Koleske[1,2,4]

[1]Interdepartmental Neuroscience Program, Departments of [2]Molecular Biophysics and Biochemistry, [3]Neurosurgery, [4]Neurobiology, [5]Psychiatry, Division of Molecular Psychiatry, Yale University, New Haven, Connecticut 06510, and [6]Department of Physiology, University of California, San Francisco, San Francisco, California 94158

Integrins are heterodimeric extracellular matrix receptors that are essential for the proper development of the vertebrate nervous system. We report here that selective loss of integrin β1 in excitatory neurons leads to reductions in the size and complexity of hippocampal dendritic arbors, hippocampal synapse loss, impaired hippocampus-dependent learning, and exaggerated psychomotor sensitivity to cocaine in mice. Our biochemical and genetic experiments demonstrate that the intracellular tail of integrin β1 binds directly to Arg kinase and that this interaction stimulates activity of the Arg substrate p190RhoGAP, an inactivator of the RhoA GTPase. Moreover, genetic manipulations that reduce integrin β1 signaling through Arg recapitulate the integrin β1 knock-out phenotype in a gene dose-sensitive manner. Together, these results describe a novel integrin β1–Arg–p190RhoGAP pathway that regulates dendritic arbor size, promotes synapse maintenance, supports proper hippocampal function, and mitigates the behavioral consequences of cocaine exposure.

Introduction

Integrins are heterodimeric (αβ) extracellular matrix (ECM) receptors that are widely expressed throughout the mammalian nervous system (Pinkstaff et al., 1999), where they are essential for several processes in neuronal development, including neural stem cell proliferation (Blaess et al., 2004; Leone et al., 2005), neuronal migration (Anton et al., 1999; Graus-Porta et al., 2001; Schmid et al., 2004; Huang et al., 2006; Belvindrah et al., 2007), cortical basal lamina formation (Graus-Porta et al., 2001), and synapse maturation and plasticity (Benson et al., 2000; Chavis and Westbrook, 2001; Huang et al., 2006; Webb et al., 2007). Integrin-mediated adhesion provides structural support for developing neurons, and culturing neurons on ligands for the β1 family of integrins increases the length and complexity of dendritic arbors (Moresco et al., 2005; Schlomann et al., 2009). Conversely, inhibiting integrin β1 signaling in developing retinal ganglion cells leads to dendrite retraction (Marrs et al., 2006), suggesting that β1-containing integrins may influence circuit function by controlling dendritic arbor formation and/or stability. Recent studies have also reported changes in expression of integrin β1 following chronic cocaine exposure (Wiggins et al., 2009), suggesting that integrin-mediated adhesion may play a protective role to stabilize neuronal structures after psychostimulant exposure (Gourley et al., 2011).

In non-neuronal cells, integrin-mediated adhesion activates the Arg nonreceptor tyrosine kinase, which phosphorylates cortactin and p190RhoGAP to promote actin rearrangements (Hernández et al., 2004b; Bradley et al., 2006; Lapetina et al., 2009). Arg is highly expressed in the brain, where it is enriched in dendritic spines (Koleske et al., 1998; Moresco et al., 2003). Although axons, dendrites, and synapses develop normally in *arg*$^{-/-}$ mice, these animals subsequently exhibit significant synapse loss and dendritic arbor atrophy in both the cortex and hippocampus by early adulthood (Moresco et al., 2005; Sfakianos et al., 2007). After synapse and dendrite loss, *arg*$^{-/-}$ mice display a number of behavioral defects, including impaired hippocampus-dependent learning and memory (Sfakianos et al., 2007), exaggerated psychomotor sensitivity to cocaine, and increased vulnerability to cocaine-induced cognitive deficits (Gourley et al., 2009).

We demonstrate here for the first time that integrin β1 signals through Arg to regulate neuronal structure in the postnatal mouse hippocampus. Conditional ablation of integrin β1 from excitatory neurons causes reductions in hippocampal synapse density and dendritic arbor size during late adolescence, coinciding with deficits in hippocampus-dependent memory tasks. In addition, we show that loss of integrin β1 from excitatory neurons in the hippocampus and cortex causes increased psychomotor sensitivity to cocaine. Using complementary biochemical and genetic approaches, we demonstrate that Arg binds directly to the

Received Aug. 1, 2011; revised Dec. 11, 2011; accepted Dec. 20, 2011.

Author contributions: M.S.W., W.D.B., S.L.G., Y.-C.L., L.F.R., C.A.G., J.R.T., and A.J.K. designed research; M.S.W., W.D.B., S.L.G., Y.-C.L., M.A.S., and A.J.K. performed research; L.F.R., C.A.G., and J.R.T. contributed unpublished reagents/analytic tools; M.S.W., W.D.B., S.L.G., Y.-C.L., and M.A.S. analyzed data; M.S.W., W.D.B., and A.J.K. wrote the paper.

This work was supported by National Research Service Award Predoctoral Awards AG039124 (M.S.W.) and NS058086 (W.D.B.) and United States Public Health Service Grants DC00210 (C.A.G.), DA011717 and AA017537 (J.R.T.), NS19090 (L.F.R.), and NS39475 and CA133346 (A.J.K.), and an Established Investigator Award from the American Heart Association (A.J.K.). We are grateful to T. Biederer and E. Robbins for advice on synaptic plasma membrane isolation, to C. Kaliszewski and X. Ye for expert technical assistance, to P. Davies for providing the anti-Arg antibody, and to D. Calderwood for critical discussions.

*M.S.W. and W.D.B. contributed equally to this work.

Correspondence should be addressed to Anthony J. Koleske, Department of Molecular Biophysics and Biochemistry, Yale University, P.O. Box 208024, New Haven, CT 06520-8024. E-mail: anthony.koleske@yale.edu.

DOI:10.1523/JNEUROSCI.3942-11.2012

 0270-6474/12/322824-11$15.00/0

β1 integrin intracellular tail and that integrin β1–Arg signaling regulates the activity of p190RhoGAP, which stabilizes dendritic arbors by inactivating the RhoA GTPase (Sfakianos et al., 2007). Together, these results identify a new role for integrin β1 *in vivo* and describe a novel integrin β1–Arg–p190RhoGAP signaling cascade that protects against synapse and dendrite loss.

Materials and Methods

Synaptic fractionation. Cortical and hippocampal homogenates were fractionated by the method of Jones and Matus (1974) with modifications (Biederer et al., 2002). Briefly, tissue was dissected from mice under deep Nembutal sedation and homogenized in ice-cold 320 mM sucrose with 10 mM HEPES, pH 7.4, in the presence of phosphatase and protease inhibitors using a glass–Teflon homogenizer. Homogenates were spun at 800 × *g* for 10 min at 4°C to clear debris, and the supernatant was collected and spun at 10,000 × *g* for 15 min at 4°C. The resulting pellet was resuspended and spun again to collect washed synaptosomes. A portion of the synaptosome fraction was separated, hypotonically lysed, and centrifuged at 24,000 × *g* for 20 min at 4°C to isolate synaptosomal membranes. Following SDS-PAGE, samples were immunoblotted with antibodies to integrin β1 (BD Biosciences) or Arg (a generous gift from Peter Davies, Albert Einstein Medical College, Bronx, NY) and detected using chemiluminescence. Quantification was performed on scanned films using Quantity One software (Bio-Rad Laboratories).

Morphometric analysis of neurons. Four hundred-micrometer-thick hippocampal slices from male mice were maintained in a standard interface chamber at 33°C. Individual live CA1 pyramidal neurons were injected with 4% biocytin in a 2 M sodium acetate solution, pH 7.5, using 300 ms current injections of 5 nA at 1 Hz for 17 min. After a 10 min recovery, injected neurons were fixed in 4% paraformaldehyde overnight, cryoprotected in 30% sucrose, resectioned at 40 μm, and visualized using standard avidin–HRP staining (Vectastain Elite ABC; Vector Laboratories). Biocytin-labeled neurons were then traced under 100× magnification using a light microscope outfitted with a *Z* drive and reconstructed using Neurolucida software by a single experimenter blinded to genotype (MicroBrightField). Sholl analysis, total dendritic length, and branchpoint number were determined using NeuroExplorer software (MicroBrightField).

Electron microscopy. Male mice were perfused transcardially under deep Nembutal anesthesia. A short (1 min) perfusion with PBS plus heparin, pH 7.4, was followed by a perfusion with 4% paraformaldehyde/0.2% glutaraldehyde in 0.1 m PBS, pH 7.4. After fixation, brains were dissected and postfixed in the same solution overnight at 4°C. Vibratome sections of the hippocampus were cut and processed in 1% OsO4 at 4°C for 1 h (Schikorski and Stevens, 1997). After dehydration in ethanol, the sections were contrasted en bloc in 0.5% uranyl acetate in 95% ethanol for 1 h and flat-embedded in Epon. Embedded vibratome sections were further cut to 70 nm thickness for electron microscopy. Sections were photographed with a JEOL 100 CX II electron microscope as 12,000× magnification. Excitatory synapses were identified in electron micrographs by the presence of a dendritic spine containing a clear electron-dense postsynaptic density apposed to an asymmetrical presynaptic compartment containing at least three synaptic vesicles (Harris and Stevens, 1989; Sfakianos et al., 2007). All measurements were made by a single experimenter blinded to the sample identity, and each mutant was matched with a wild-type (WT) littermate control. Dendritic spine head area was measured using ImageJ in spines with a clearly visible neck and measured from the thinnest part of the neck.

Cloning. The cytoplasmic tail of integrin β1 (amino acids 752–798) was subcloned from cDNA (ATCC; accession number BC020057) into pGEX-4T1 (GE Healthcare). An α-helical linker to separate the globular GST moiety from the β1 tail was subcloned from the Bcr protein (amino acids 1–68).

Protein purification and bead coupling. His-tagged recombinant full-length Arg, ArgΔC (amino acids 1–557), Arg557-C (amino acids 557–1182), and Arg kinase domain (amino acids 281–557) were produced in baculovirally infected Hi5 insect cells (Invitrogen) as previously described (Lapetina et al., 2009). GST-tagged recombinant Arg SH3SH2 (amino acids 112–254) was produced in Rosetta cells by inoculating culture, and then inducing protein expression with the addition of 0.25 mM IPTG (isopropyl β-D-thiogalactoside) overnight. Cells were centrifuged, resuspended in 50 mM Tris, pH 8, 150 mM NaCl, 10% glycerol, 1 mM DTT, 5 mM EDTA, and protease inhibitors, passed through French Press, and lysed with 1% Triton X-100. Following clarification, lysates were incubated with glutathione-agarose beads (Sigma-Aldrich) for 1 h, applied to column, washed with 10 vol of Wash A (50 mM Tris, pH 8, 500 mM NaCl, 5% glycerol, 1 mM DTT, 0.01% Triton X-100, 1 mM PMSF), then 10 vol of Wash B (Wash A with 100 mM NaCl), and then eluted in Wash B plus 10 mM glutathione. The GST tag was removed with PreScission Protease (GE Healthcare) following the manufacturer's protocol. GST-linker and GST-β1 integrin tails were purified as above, without GST tag cleavage. Full-length Arg, ArgΔC, Arg557-C, Arg kinase domain, and SH3SH2 were dialyzed into 36.5 mM phosphate buffer, pH 7.4, 500 mM NaCl, and coupled to AminoLink beads (Pierce) according to the manufacturer's protocol at a final concentration of 100 μM. Beads were blocked with BSA and 1 M Tris, then washed, and stored in 50% glycerol.

Binding assays. The 1 μM Arg or Arg fragments coupled to beads were incubated with varying concentrations of GST-β1 tail or GST-linker control in binding buffer (25 mM HEPES, pH 7.25, 100 mM NaCl, 5% glycerol, 0.01% Triton X-100, 1 mM DTT) for 1 h at 4°C with gentle mixing. Reactions were centrifuged at 16,000 × *g*, and pellets were washed twice with binding buffer, before resuspension in sample buffer. Samples were separated on 10% BIS-Tris gels using MOPS (4-morpholinepropanesulfonic acid) running buffer, stained with Coomassie R-250 (Pierce), and then scanned and quantitated using ImageQuant software (Bio-Rad).

Neuronal culture and imaging. Primary neuronal cultures were prepared from postnatal day 0 mouse hippocampi. Neurons were dissociated and plated at density of 0.3×10^6 cells/ml on glass coverslips coated with poly-D-lysine (20 μg/ml; BD Biosciences). Cultures were maintained in serum-free media containing 1% penicillin/streptomycin, 1% L-glutamine, and 2% B27 supplement (Invitrogen) in neural basal media (Invitrogen). Neurons were transfected with Arg-RFP and β1 integrin-GFP at 7 d *in vitro* (DIV), fixed, and immunostained at 15 DIV. Images were taken using a LSM710 confocal microscope (Zeiss) at 63x objective.

Immunoprecipitations. Integrin β1 was immunoprecipitated from Triton X-100 (1%)-solubilized brain membrane extracts in the presence of protease and phosphatase inhibitors (Dulabon et al., 2000). Protein extract (0.5 mg; standardized to 1 mg/ml) was precleared with 40 μl of Protein G Plus/A-Agarose beads (Calbiochem) for 20 min at 4°C. The precleared supernatant was then incubated with 40 μl of beads that had been incubated for 12 h with anti-integrin β1 antibody (BD Biosciences) for 1 h at 4°C with gentle mixing. Immunoprecipitates were washed three times with 1 ml of lysis buffer, suspended in 40 μl of sample buffer, and separated by SDS-PAGE for immunoblot analysis. Coimmunoprecipitated proteins and loading controls were detected by stripping and reprobing the blot with anti-integrin β1 and anti-Arg antibodies.

For p190RhoGAP immunoprecipitations, hippocampi were dissected from male mice in ice-cold PBS and homogenized in lysis buffer (20 mM Tris, pH 7.5, 150 mM NaCl, 2 mM EDTA, 1% Triton X-100, and protease and phosphatase inhibitors). Protein extract (0.5 mg; standardized to 1 mg/ml) was precleared with 40 μl of Protein G Plus/A-Agarose beads (Calbiochem) for 20 min at 4°C. The precleared supernatant was then incubated with 2 μg of anti-p190RhoGAP monoclonal antibody (Millipore) overnight at 4°C with gentle mixing. Forty microliters of Protein G Plus/A-Agarose beads (preequilibrated) were then added, and immune complexes were incubated for 1 h at 4°C with gentle mixing. Immunoprecipitates were washed three times with 1 ml of lysis buffer, suspended in 40 μl of sample buffer, and separated by SDS-PAGE for immunoblot analysis. Coimmunoprecipitated proteins and loading controls were detected by stripping and reprobing the blot with anti-120RasGAP (Millipore) and anti-p190RhoGAP (BD Biosciences) antibodies. Bands were quantified using a densitometer and ImageQuant software, and the relative amount of coimmunoprecipitated protein was standardized to WT littermate controls run on the same blot.

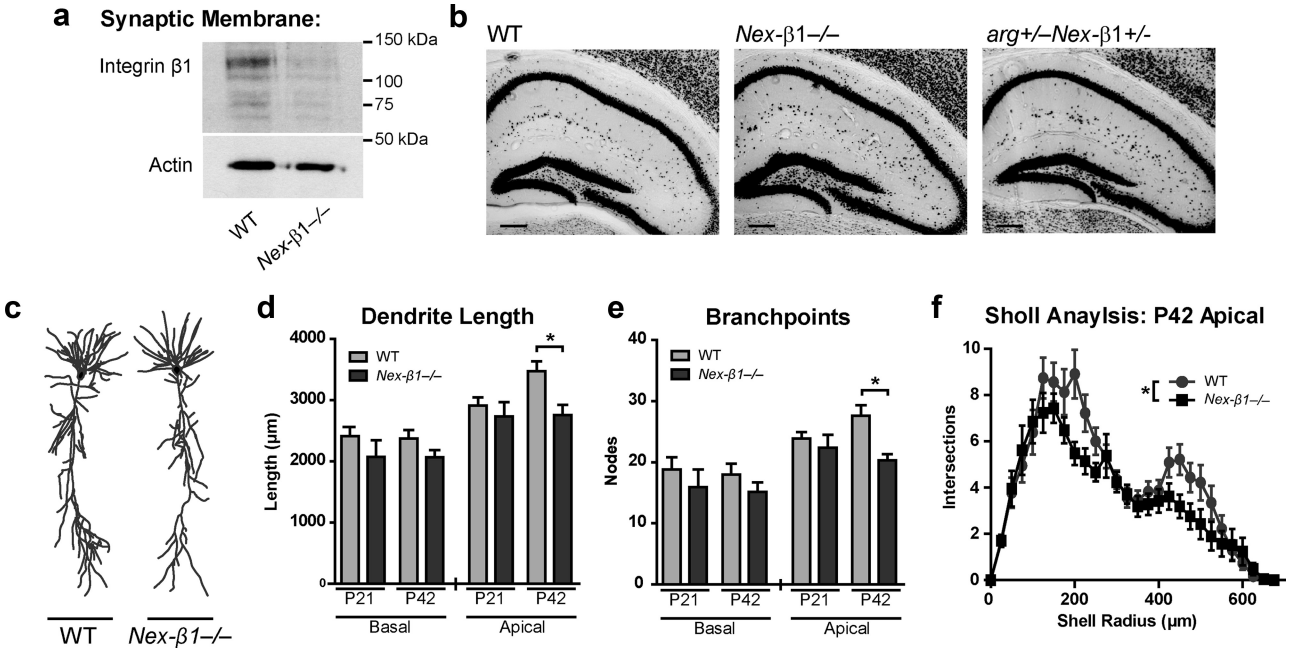

Figure 1. Dendritic arbors fail to elaborate in *Nex-β1*$^{-/-}$ mice. ***a***, Immunoblot demonstrating that integrin β1 expression levels are significantly reduced in *Nex-β1*$^{-/-}$ forebrain synaptic membrane fractions versus WT at P42. ***b***, NeuN immunohistochemistry of P42 hippocampal sections. Staining reveals no apparent differences in overall hippocampal ultrastructure in *Nex-β1*$^{-/-}$ or *arg*$^{+/-}$*Nex-β1*$^{+/-}$ versus WT mice. Scale bar, 200 μm. ***c***, Representative dendritic reconstructions of WT and *Nex-β1*$^{-/-}$ hippocampal neurons at postnatal day 42. ***d***, ***e***, Mean total dendritic length (***d***) and branch point number (***e***) of basal (left) and apical (right) dendritic arbors of CA1 hippocampal neurons. Apical dendritic arbors *Nex-β1*$^{-/-}$ mice exhibited reductions in both length and branch point number relative to WT at P42. Student's *t* test, length, $p = 0.004$; branch point, $p = 0.001$. $n = 13$–24 neurons for each group. ***f***, Sholl analysis of P42 dendrites from the same reconstructions revealed a reduction in *Nex-β1*$^{-/-}$ neurons throughout the apical arbor. Main effect of genotype, ANOVA ($F_{(1,27)} = 4.366$; $p = 0.04$). Values represent mean ± SEM. *$p < 0.05$ throughout.

Rho activity assays. Rho activity assays were performed from hippocampal samples using an ELISA-based assay (Cytoskeleton) as described previously (Bradley et al., 2006).

Novel object recognition task. Object recognition tests were conducted in a lit, quiet room using 7-week-old male mice as previously described (Sfakianos et al., 2007). Briefly, mice were placed in a large, clean field (41 × 20 cm) and allowed to explore two identical objects placed at opposite ends of the field for a total of 30 s. Forty-eight hours later, mice were placed in the same field, and time spent exploring one familiar and one novel object was quantified until animals had accumulated 30 s of exploration time. Mice that did not explore the objects for a total of 30 s within 5 min were excluded. Exploration was defined as nasal or oral contact with the objects, and raters blinded to mouse genotype scored all sessions.

Cocaine administration. Male adult mice were injected with cocaine hydrochloride (10 mg/kg, i.p.; 1 ml/100 g; generously provided by NIDA) after 1 h habituation to a large, clean cage normally used to house rats (41 × 20 × 20 cm) that was placed in Omnitech Digiscan Micromonitor frames equipped with 16 photocells. The number of photobeam breaks generated during the 30 min after cocaine administration was normalized to each animal's own baseline.

Reversal learning. A spatial reversal learning task sensitive to hippocampal lesions was conducted using methods similar to those previously described (Gourley et al., 2010); food-restricted male mice were trained to nose poke for food reinforcement (20 mg grain pellets; Bio-Serv) in standard MED Associates conditioning chambers equipped with three stationary nose poke recesses. Nose poke training was initiated with training sessions during which mice were reinforced for entering the nose into a single designated recess, and each response was reinforced until animals earned 30 pellets or 135 min elapsed. All mice acquired the response within five daily sessions, with no differences in response acquisition. Then, the location of the reinforced aperture within the chamber was "reversed," such that a mouse trained to respond on the leftmost aperture was now reinforced for responding on the rightmost aperture or vice versa. Again, the session ended when mice acquired 30 pellets or 135 min elapsed, and errors (responses made on the previously reinforced aperture) were quantified during two sessions.

Statistics. All data are reported as mean ± SEM. Comparisons between WT and *Nex-β1*$^{-/-}$ mice were performed with two-tailed Student's *t* tests. For all comparisons with multiple mutant genotypes, a one-way ANOVA was performed to determine whether the genotype had a statistically significant overall effect, and *post hoc* statistical comparisons were performed with two-tailed Student's *t* tests. For RhoA activity assays, experimental samples were standardized to WT littermate samples run during the same assay to reduce interassay error, and datasets were analyzed using a one-sample *t* test comparing the mean to a value of 1. Datasets were also analyzed by two-factor (Sholl analysis, cocaine sensitivity, reversal learning) or three-factor (novel object recognition) ANOVA. Statistics were performed with GraphPad Prism (GraphPad Software).

Results

Deletion of integrin β1 in hippocampal neurons compromises dendritic arbor size

We inactivated integrin β1 expression by crossing mice containing a floxed allele of the gene encoding β1 (*itgb1*) (Graus-Porta et al., 2001) with NEX-Cre transgenic mice that express Cre recombinase selectively in excitatory forebrain neurons in the forebrain (Goebbels et al., 2006). This combination efficiently inactivates *itgb1* in excitatory neurons of the cortex and hippocampus beginning at approximately embryonic day 11.5 (E11.5) (Belvindrah et al., 2007). For simplicity, mice expressing one copy of the floxed *itgb1* allele and NEX-Cre (*itgb1*$^{+/flox}$ NEX-Cre^{+}) will be referred to as *Nex-β1*$^{+/-}$, while mice carrying two copies of the floxed *itgb1* allele and NEX-Cre (*itgb1*$^{flox/flox}$ NEX-Cre^{+}) will be referred to as *Nex-β1*$^{-/-}$. Quantitative immunoblotting revealed that integrin β1 levels were reduced by >80% in hippocampal synaptic membrane fractions from *Nex-β1*$^{-/-}$ mice (Fig. 1a).

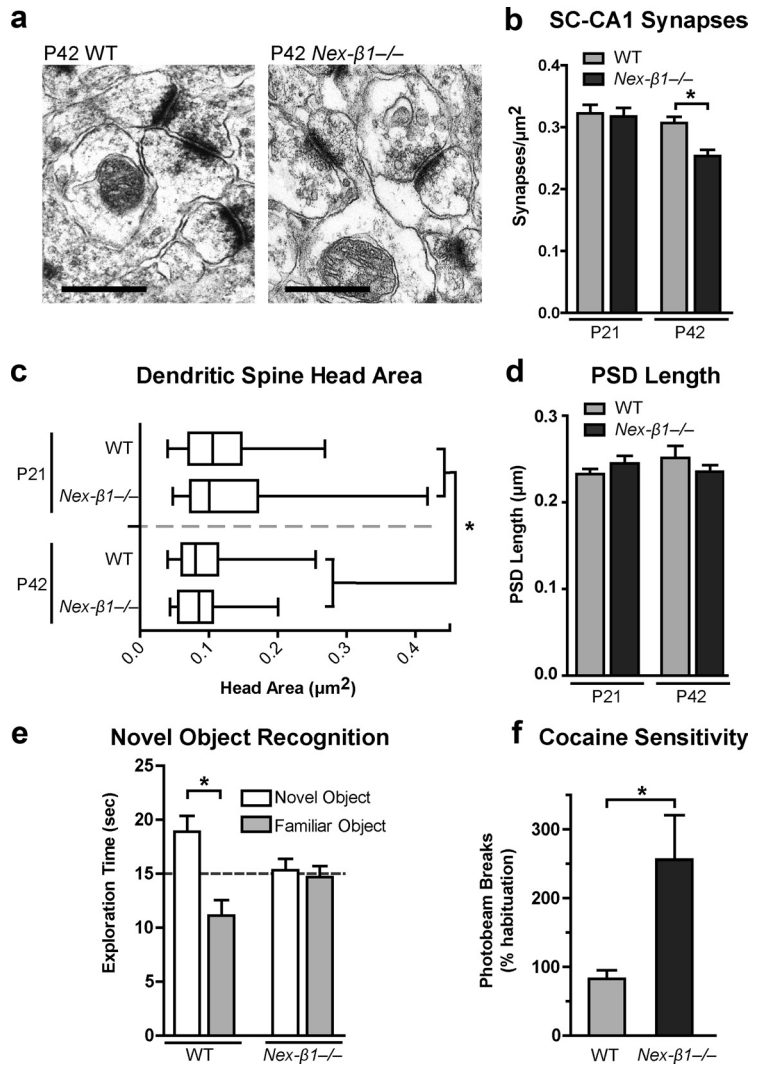

Figure 2. P42 *Nex-β1*$^{-/-}$ mice have reduced hippocampal synaptic density and exhibit behavioral deficits. ***a***, Representative electron micrographs of excitatory synaptic contacts in the CA1 region of the WT (left) and *Nex-β1*$^{-/-}$ P42 hippocampus. Scale bar, 500 nm. ***b***, Mean SC–CA1 synapse density in WT and *Nex-β1*$^{-/-}$ mice at P21 and P42. Synapse density was reduced in *Nex-β1*$^{-/-}$ mice relative to WT at P42, but not at P21. Student's *t* test, $p < 0.001$. For P21, $n = 30$ sections, 2 mice for each genotype; P42 WT, $n = 94$ sections, 6 mice; P42 *Nex-β1*$^{-/-}$, $n = 51$ sections, 3 mice. ***c***, Measurement of dendritic spine head size at P21 and P42. Main effect of age on size, ANOVA (age by genotype) ($F = 10.34$; $p = 0.0015$). $n = 53$–78 spines per group, 2–3 mice. ***d***, PSD length is unaltered in *Nex-β1*$^{-/-}$ mice. $n = 80$–160 measurements per group, 2–3 mice. ***e***, Performance of P42 WT and *Nex-β1*$^{-/-}$ mice in an object recognition task. Time spent exploring two objects, one novel and one familiar, is quantified. WT mice spent more time exploring the novel object, but *Nex-β1*$^{-/-}$ mice showed no significant preference between the novel and familiar object. Genotype by object interaction, ANOVA ($F_{(1,28)} = 6.0$; $p = 0.02$), Student's *post hoc t* tests, $p < 0.05$. $n =$ 6–10 mice per group. ***f***, Locomotor response to acute injection of 10 mg/kg cocaine. Cocaine sensitivity was heightened in *Nex-β1*$^{-/-}$ adult mice relative to WT. Student's *t* test, $p < 0.001$. $n = 3$–6 mice per group, >8 weeks of age. Values represent mean ± SEM. *$p < 0.05$ throughout.

The residual integrin β1 in the synaptic membrane fractions of *Nex-β1*$^{-/-}$ mice may reflect inadequate *itgb1* recombination in a limited subset of neurons or contamination of the hippocampal synaptic membrane fraction by integrin β1 present in inhibitory neurons and glia. Both *Nex-β1*$^{+/-}$ and *Nex-β1*$^{-/-}$ mice were visually indistinguishable from WT littermates (data not shown), and we did not detect any differences in hippocampal ultrastructure (Fig. 1b) or cortical lamination in *Nex-β1*$^{-/-}$ mice compared with WT mice, in agreement with previously published results (Belvindrah et al., 2007).

We used live-cell labeling of hippocampal CA1 pyramidal neurons in acute slices followed by 3D reconstruction and morphometric analysis to quantitatively assess dendritic structure in *Nex-β1*$^{-/-}$ mice (Fig. 1*c*). Apical dendritic arbors developed normally in *Nex-β1*$^{-/-}$ mice through postnatal day 21 (P21), but at P42 were reduced by 21% in length (Fig. 1*d*) and had a 26% reduction in the number of branch points (Fig. 1*e*) compared with WT littermates. Sholl analysis (Sholl, 1953) revealed that these reductions were distributed throughout the dendritic arbor (Fig. 1*f*). The length and branch point number of basal dendritic arbors were not significantly different from WT in *Nex-β1*$^{-/-}$ mice at either P21 or P42 (Fig. 1*d*,*e*).

Loss of integrin β1 reduces hippocampal synapse density and causes behavioral deficits

We next examined whether the density of Schaffer collateral–CA1 (SC–CA1) synapses (Fig. 2*a*), which form on the apical arbors of CA1 pyramidal neurons, was altered in *Nex-β1*$^{-/-}$ mice. As with dendritic arbors, SC–CA1 synapse density was similar to WT in *Nex-β1*$^{-/-}$ mice at P21 but was reduced by 23% at P42 (Fig. 2*b*). As a measure of dendritic spine morphology, we measured spine head area and postsynaptic density (PSD) length in spines from WT and *Nex-β1*$^{-/-}$ mice. In agreement with previously published results (Sfakianos et al., 2007), we observed a broad distribution of spine head sizes at P21, which reduced in size by P42. No significant differences were observed in head size or PSD length in *Nex-β1*$^{-/-}$ mice at either age.

Given the hippocampal synapse and dendrite loss observed in *Nex-β1*$^{-/-}$ mice, we tested whether hippocampal function was compromised by measuring performance in a hippocampus-dependent novel object recognition task that we have previously used to characterize behavioral deficits in *arg*$^{-/-}$ mice (Moresco et al., 2005). Forty-eight hours after exposure to two identical objects, P42 mice were placed into a test cage with one object identical with the previously explored objects and one novel object. WT mice showed a significant preference for the novel object, indicating memory for the familiar one (Fig. 2*e*). By contrast, *Nex-β1*$^{-/-}$ mice failed to discriminate between the novel and familiar objects (Fig. 2*e*). Thus, the reduction in synapses and dendritic arbors are accompanied by impairments in a hippocampus-dependent task.

Cocaine exposure alters integrin β1 expression (Wiggins et al., 2009), but the effect of integrin signaling on cocaine sensitivity in excitatory hippocampal and cortical neurons has not been directly tested. Therefore, we compared the psychomotor response to a low dose (10 mg/kg, i.p.) of cocaine in adult WT and *Nex-β1*$^{-/-}$ mice. In agreement with previous reports (Gourley et al.,

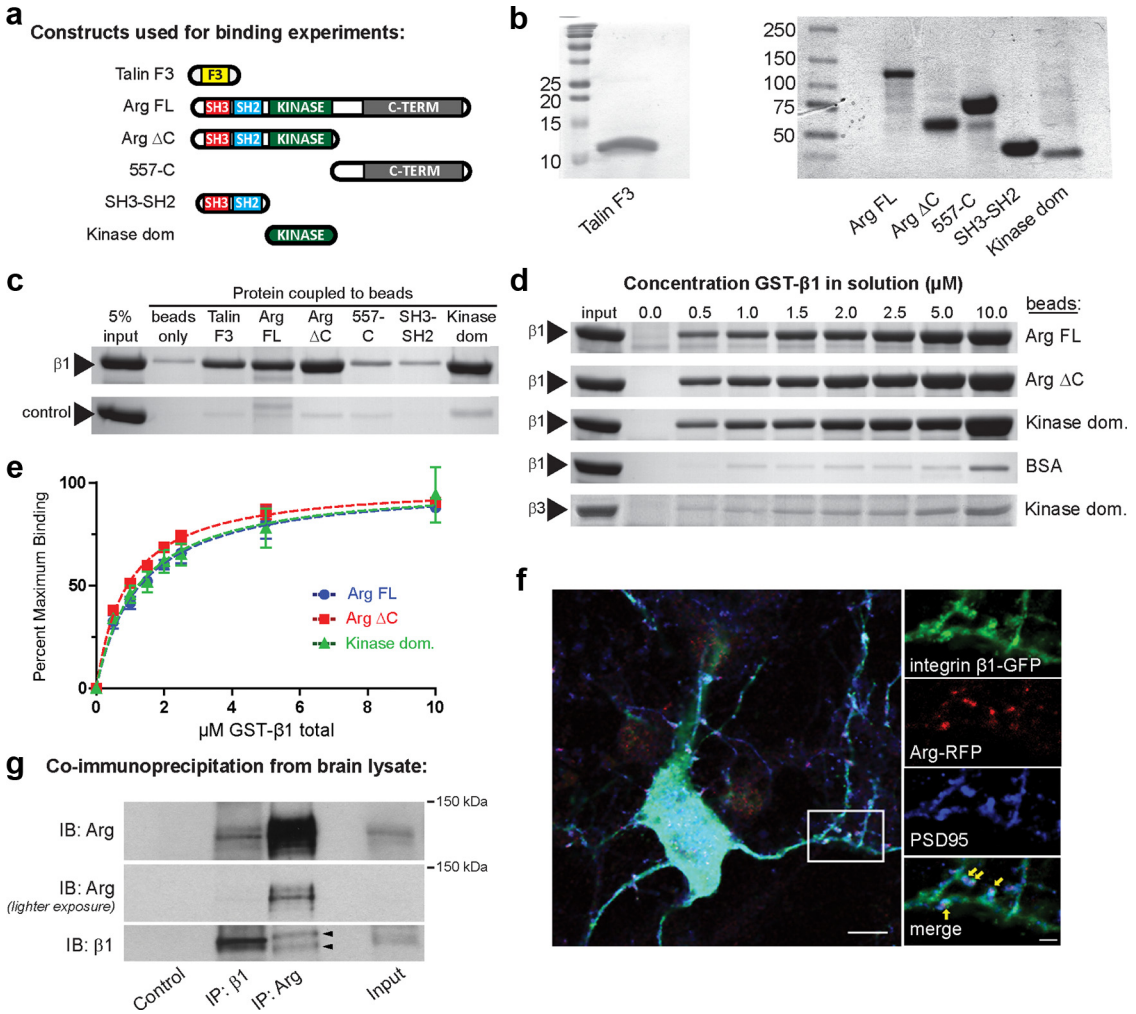

Figure 3. Integrin β1 interacts directly with Arg. ***a***, Diagram of protein constructs used for binding experiments. ***b***, Representative protein gels showing purity of proteins used for binding experiments. Gels were loaded with 5 μg of purified protein and stained with Coomassie G-250 stain. Note that the Talin F3 construct was run on a separate 20% gel due to its small size. The band representing the SH3–SH2 contains a GST tag that was removed before running binding experiments. ***c***, Protein gel showing soluble GST-tagged β1 tails (top panel) or a GST-linker control (bottom panel) binding to AminoLink beads covalently coupled to either BSA (negative control), the Talin F3 domain, Arg FL (full-length Arg), ArgΔC (residues 1–557), Arg 557-C, the Arg SH3–SH2 domains, or Arg kinase domain. GST-β1 bound to the positive control (Talin F3) and to Arg, ArgΔC, and the Arg kinase domain. GST-β1 did not bind to Arg 557-C or the Arg SH3–SH2 domains significantly above background. The Arg kinase domain was sufficient for binding to integrin β1. ***d***, Protein gel showing concentration-sensitive binding of GST-β1 to beads coupled to Arg FL, ArgΔC, or the Arg kinase domain. The Arg kinase domain did not bind appreciably to GST-β3. ***e***, Plot of ***d*** normalized to the maximal binding (B_{max}). Calculated binding affinities are as follows: Arg FL $K_d = 1.29 \pm 0.20$ μM, ArgΔC $K_d = 0.92 \pm 0.08$ μM, kinase domain $K_d = 1.23 \pm 0.26$ μM. ***f***, Localization of fluorescently tagged functional Arg (Arg-RFP) and β1 integrin (β1-GFP) expressed in cultured hippocampal neurons at 15 DIV along with immunofluorescence staining for PSD95. Arg-RFP and β1-GFP partially colocalized with PSD95 at dendritic spines, as highlighted by arrows. Scale bars: large image, 10 μm; inset, 2 μm. The box indicates region of inset. ***g***, Immunoprecipitations of integrin β1 and Arg from forebrain lysates. Control lane represents protein-A/G beads that have been treated with an equivalent volume of rabbit serum; input lane is 10% of total protein. A fraction of Arg coimmunoprecipitated with antibodies against integrin β1. Significant levels of integrin β1 were not detected in the Arg immunoprecipitation; the arrowheads denote nonspecific bands that are remain present when only secondary antibodies are applied.

2009), this dose did not affect locomotion in WT mice; however, it significantly heightened locomotor activity in *Nex-β1*$^{-/-}$ mice (Fig. 2f), indicating that these mice are more sensitive to the stimulant properties of cocaine.

Integrin β1 localizes to dendritic spines and binds directly to Arg

The *Nex-β1*$^{-/-}$ phenotype closely resembles that previously described in *arg*$^{-/-}$ mice, in which hippocampal synapses and dendrites develop normally through P21 but are reduced at P42 (Sfakianos et al., 2007). Adhesion of fibroblasts and cultured cortical neurons to extracellular matrix proteins triggers Arg-mediated phosphorylation of p190RhoGAP (Hernández et al., 2004a; Bradley et al., 2006; Peacock et al., 2007) and cortactin (Lapetina et al., 2009), suggesting that integrins stimulate Arg activity.

Integrin β intracellular tails bind directly to and activate several signaling partners, including Src family kinases (Arias-Salgado et al., 2003; Harburger and Calderwood, 2009). To test whether the integrin β1 tail also binds directly to Arg, we covalently coupled purified recombinant Arg or Arg fragments (Fig. 3*a*,*b*) to beads and measured their ability to bind to a protein fusion comprised of glutathione *S*-transferase, a short linker, and the integrin β1 tail (GST-β1). Full-length Arg bound to the GST-β1 tail in a concentration-dependent saturable manner, while a GST-linker control protein did not exhibit significant binding to Arg (Fig. 3*a*–*e*). Both Src and Abl family kinases contain Src homology 3 (SH3), SH2, and kinase domains, and Src

employs its SH3 domain to bind the integrin β3 cytoplasmic tail (Arias-Salgado et al., 2003). Therefore, we tested whether Arg uses its SH3 domain to engage integrin β1. Surprisingly, a construct containing only the SH3 and SH2 domains did not bind to GST-β1 appreciably above background (Fig. 3*c*), while the Arg kinase domain alone was sufficient for high-affinity binding to β1 (Fig. 3*a–e*). The kinase domain bound to GST-β1 with similar affinity to full-length Arg (Fig. 3*e*; Arg FL $K_d = 1.29 \pm 0.20$ μM, Arg kinase domain $K_d = 1.23 \pm 0.26$ μM). We also tested the specificity of the interaction by measuring whether the Arg kinase domain also binds to the tail of integrin β3. The kinase domain did not bind appreciably to GST-β3 (Fig. 3*d*, estimated $K_d > 10$ μM), indicating that the integrin β1-Arg interaction is specific.

To test whether the proteins have the potential to interact in neurons, we coexpressed functional fluorescently protein-tagged versions of Arg (Arg-RFP) and integrin β1 (β1-GFP) in cultured hippocampal neurons and examined their localization at 15 DIV. Arg-RFP was significantly enriched in dendritic spines, as identified by staining for the postsynaptic protein PSD95 (Fig. 3*f*), in agreement with previous immunolocalization studies (Koleske et al., 1998; Moresco et al., 2003). β1-GFP localized throughout the dendritic arbor, but was also present in dendritic spines, where a portion colocalized with Arg-RFP and PSD95 (Fig. 3*f*). Expression of β1-GFP in WT neurons did not affect overall dendritic length ($n = 15$–16 neurons; $p = 0.83$), dendritic branch number ($n = 15$–16 neurons; $p = 0.26$), or dendritic spine density ($n = 13$–17 neurons; $p = 0.91$). Similarly, expression of Arg-RFP does not alter dendritic morphology or spine density (Y.-C. Lin and A. J. Koleske, unpublished observations). Arg also coimmunoprecipitated with integrin β1 from cortical and hippocampal tissue (Fig. 3*g*). Together, these binding, localization, and coimmunoprecipitation studies demonstrate that β1 integrin interacts with Arg and that both proteins localize to dendritic spines, suggesting that β1 integrin may signal directly through Arg in dendritic spines *in vivo*.

Integrin β1–Arg signaling acts via p190RhoGAP to attenuate RhoA activity

p190RhoGAP is a major inactivator of the RhoA GTPase and is a substrate of Arg in the brain, where Arg and p190RhoGAP interact genetically to regulate dendritic arbor size (Hernández et al., 2004b; Sfakianos et al., 2007). The relative amounts of Arg and its downstream signaling partners p190RhoGAP and p120RasGAP were unchanged in synaptoneurosomal fractions from *Nex-β1*$^{-/-}$ mice relative to WT mice, indicating that integrin β1 was not essential for localization of these signaling components to synapses (Fig. 4*a*). Arg-mediated phosphorylation of p190RhoGAP promotes its binding to p120RasGAP, which is required for its recruitment to the membrane where it can target active RhoA (Parsons, 1996; Arthur et al., 2000; Hernández et al., 2004b; Bradley et al., 2006; Peacock et al., 2007). Therefore, the relative amount of p120RasGAP bound to p190RhoGAP is used as a measure of p190RhoGAP activity (Hernández et al., 2004b; Bradley et al., 2006; Sfakianos et al., 2007). We used immunoprecipitation to measure p120RasGAP:p190RhoGAP complex levels and p190RhoGAP phosphorylation in hippocampal extracts (Fig. 4*b–e*). In P21 animals, the amount of p120RasGAP bound to p190RhoGAP was similar in WT, *arg*$^{+/-}$, *Nex-β1*$^{+/-}$, *arg*$^{+/-}$*Nex-β1*$^{+/-}$, and *Nex-β1*$^{-/-}$ mice. At P42, however, the level of p120RasGAP:p190RhoGAP complex was significantly reduced in *arg*$^{+/-}$*Nex-β1*$^{+/-}$, and *Nex-β1*$^{-/-}$ mice relative to WT, indicative of reduced p190RhoGAP activity (Fig. 4*b*,*c*). Consistent with this result, p190RhoGAP phosphorylation levels were also reduced in *arg*$^{+/-}$*Nex-β1*$^{+/-}$, and *Nex-β1*$^{-/-}$ mice at P42, but not at P21 (Fig. 4*d*,*e*). These results demonstrate that integrin β1 is required for optimal p190RhoGAP activation and that *itgb1* and *arg* interact in a gene dose-dependent manner to regulate p190RhoGAP activity. Together with the binding experiments showing a physical interaction between integrin β1 and Arg, these results strongly suggest that integrin β1 and Arg interact functionally to regulate p190RhoGAP activity *in vivo*.

To confirm that the decrease in p120RasGAP:p190RhoGAP complex formation represented decreased p190RhoGAP activity, we measured hippocampal RhoA activity in WT, *arg*$^{+/-}$*Nex-β1*$^{+/-}$, and *Nex-β1*$^{-/-}$ mice. Consistent with the reduced levels of p120RasGAP:p190RhoGAP complex, hippocampal RhoA activity was significantly increased in *arg*$^{+/-}$*Nex-β1*$^{+/-}$ and *Nex-β1*$^{-/-}$ mice at P42 relative to WT littermate controls (Fig. 4*f*), but were not significantly different from WT at P21. Elevated RhoA signaling antagonizes dendrite development and stability in a wide range of contexts (Threadgill et al., 1997; Van Aelst and Cline, 2004). Importantly, both the decrease in p120RasGAP:p190RhoGAP complex formation and resultant increase in RhoA activity were age dependent and followed the same timeline as the reductions in synapse number and dendrite size seen in *arg*$^{-/-}$ (Sfakianos et al., 2007) and *Nex-β1*$^{-/-}$ mice (Figs. 1*d–f*, 2*b*).

Arg interacts functionally with integrin β1 to regulate dendritic structure and synapse density

Having established that integrin β1 and Arg interact functionally to regulate p190RhoGAP signaling, we used dose-sensitive interactions to test whether this interaction regulates dendritic arbor size and synapse number. Hippocampal CA1 pyramidal neurons from *arg*$^{+/-}$ and *Nex-β1*$^{+/-}$ mice had apical dendritic arbors that were indistinguishable in length (Fig. 5*a*) and branch point number (Fig. 5*b*) from control WT littermates at both P21 and P42. In contrast, although similar to WT at P21, apical dendritic arbors in *arg*$^{+/-}$*Nex-β1*$^{+/-}$ double heterozygotes were 18% shorter in length and had 24% fewer branch points than WT at P42 (Fig. 5*a*,*b*). Importantly, the time course, magnitude, and distribution (Fig. 5*c*) of these reductions were similar to those observed in *arg*$^{-/-}$ (Sfakianos et al., 2007) and *Nex-β1*$^{-/-}$ mice (Fig. 1*c–f*). Together with the interaction data presented above, these data strongly suggest that integrin β1 signals through Arg to stabilize hippocampal dendritic arbors. *arg*$^{+/-}$ mice were also crossed with mice harboring a heterozygous deletion of *itgb3* (integrin β3) as an additional control. No reduction in dendritic arbor size or branch point number was observed in mice doubly heterozygous for germline mutations in *arg* and *integrin β3* (*arg*$^{+/-}$*β3*$^{+/-}$) (Fig. 5*a*,*b*), suggesting that Arg may interact selectively with integrin β1.

We also measured the density of SC–CA1 synapses in *arg*$^{+/-}$*Nex-β1*$^{+/-}$ mice via electron microscopy. As in *Nex-β1*$^{-/-}$ mice, SC–CA1 synapse density in *arg*$^{+/-}$*Nex-β1*$^{+/-}$ mice was identical with WT at P21, but was reduced by 28% at P42 (Fig. 5*d*). These reductions are similar in magnitude to the synapse loss observed in *arg*$^{-/-}$ mice at P42 (Sfakianos et al., 2007).

Integrin β1–Arg signaling regulates behavior

We tested the behavioral consequence of reduced integrin β1:Arg signaling using the novel object recognition task. While WT, *arg*$^{+/-}$, and *Nex-β1*$^{+/-}$ P42 mice all exhibited a significant preference for the novel object (Fig. 5*e*), *arg*$^{+/-}$*Nex-β1*$^{+/-}$ mice failed to discriminate between the novel and familiar objects (Fig. 5*e*), a similar deficit to that observed in both *arg*$^{-/-}$ and *Nex-*

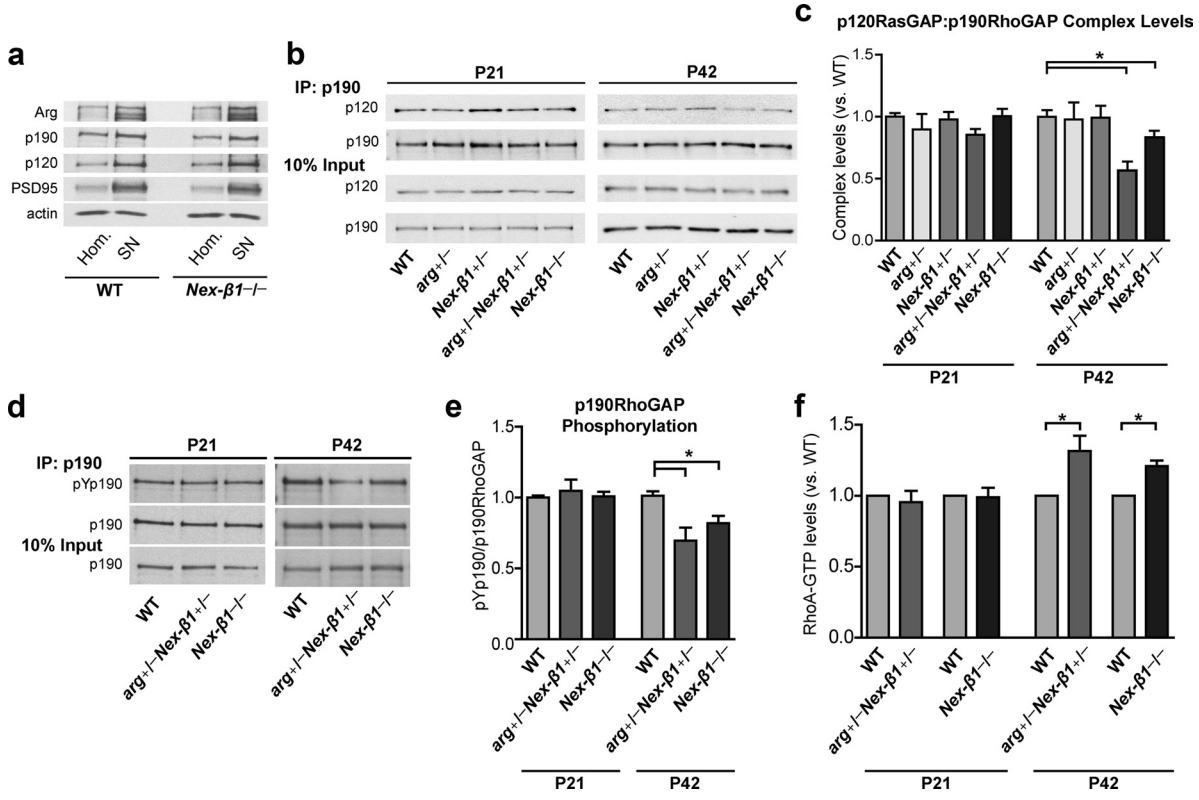

Figure 4. Integrin β1–Arg signaling regulates p190RhoGAP activity. ***a***, Immunoblot showing enrichment of Arg, p190RhoGAP (p190) and p120RasGAP (p120) in synaptoneurosomal fractions prepared from both WT and *Nex-β1* $^{-/-}$ mice. PSD95 and actin are included as loading controls. ***b***, Representative examples of p190 immunoprecipitation with coimmunoprecipitated p120. ***c***, Quantification of p120RasGAP:p190RhoGAP complex. Complex level values represent p120 signal standardized to the amount of p190 in each IP compared with WT littermates. *arg* $^{+/-}$*Nex-β1* $^{+/-}$ and *Nex-β1* $^{-/-}$ mice had significantly lower levels of p120RasGAP:p190RhoGAP complex than WT at P42. One-way ANOVA revealed no significant difference between genotypes at P21, but a significant effect of genotype at P42 ($F_{(4,34)} = 3.856$; $p = 0.011$). p120RasGAP:p190RhoGAP complex levels were reduced at P42 in both *arg* $^{+/-}$*Nex-β1* $^{+/-}$ and *Nex-β1* $^{-/-}$ mice. Student's *post hoc t* test versus WT, P42 *arg* $^{+/-}$*Nex-β1* $^{+/-}$, $p = 0.001$; P42 *Nex-β1* $^{-/-}$, $p = 0.049$, $n = 7$–14 mice for each genotype. ***d***, Representative examples of phospho-p190RhoGAP (pYp190) measurement from a p190 immunoprecipitation. ***e***, Quantification of p190RhoGAP phosphorylation levels from WT and mutant mice. One-way ANOVA revealed no significant difference between genotypes at P21, but a significant effect of genotype at P42 ($F_{(2,16)} = 8.379$; $p = 0.0032$), with decreased pYp190 levels in both *arg* $^{+/-}$*Nex-β1* $^{+/-}$ and *Nex-β1* $^{-/-}$ mice. Student's *post hoc t* test versus WT, P42 *arg* $^{+/-}$*Nex-β1* $^{+/-}$, $p = 0.002$; P42 *Nex-β1* $^{-/-}$, $p = 0.007$; $n = 4$–8 mice for each genotype. ***f***, Quantification of Rho activity in *arg* $^{+/-}$*Nex-β1* $^{+/-}$ and *Nex-β1* $^{-/-}$ mice. The amount of active Rho-GTP from each mutant mouse was compared with a WT littermate run in the same assay. Both *arg* $^{+/-}$*Nex-β1* $^{+/-}$ and *Nex-β1* $^{-/-}$ mice had increased hippocampal Rho activity. One-sample *t* test comparing means to 1, P42 *arg* $^{+/-}$*Nex-β1* $^{+/-}$, $p = 0.02$; P42 *Nex-β1* $^{-/-}$, $p = 0.03$. $n = 3$–7 mice per group. Values represent mean ± SEM. $^*p < 0.05$ throughout.

β1 $^{-/-}$ mice (Fig. 2*e*). As an additional test of hippocampal function, mice were tested in a spatial reversal learning task (Gourley et al., 2010). Mice initially trained to enter their noses into a specific recess to earn food rewards were required to redirect responding to a new reinforced recess. WT, *arg* $^{+/-}$, and *Nex-β1* $^{+/-}$ mice did not differ in the number of errors committed. As in the novel object recognition task, however, *arg* $^{+/-}$*Nex-β1* $^{+/-}$ mice were significantly impaired, committing substantially more errors than all other groups (Fig. 5*f*). Thus, *arg* $^{+/-}$*Nex-β1* $^{+/-}$ mice are impaired in two distinct behavioral tasks that are sensitive to hippocampal defects.

Both *arg* $^{-/-}$ (Gourley et al., 2009) and *Nex-β1* $^{-/-}$ (Fig. 2*f*) mice display heightened psychomotor sensitivity to cocaine. To determine whether the integrin β1–Arg interaction affects cocaine sensitivity, we also measured the psychomotor response to low-dose cocaine (10 mg/kg, i.p.) in adult mice with differing *arg* or *itgb1* gene dosage. This dose of cocaine had no effect on locomotion in WT, *arg* $^{+/-}$, or *Nex-β1* $^{+/-}$ mice, but *arg* $^{+/-}$*Nex-β1* $^{+/-}$ mice exhibited greatly increased locomotion after exposure (Fig. 5*g*), demonstrating a functional interaction between integrin β1 and Arg that mitigates against the stimulant properties of cocaine.

Discussion

We report here that loss of integrin β1 function in excitatory hippocampal neurons leads to reductions of apical dendritic arbor size in the CA1 stratum radiatum, synapse loss, and behavioral deficits. Our biochemical and genetic experiments indicate that integrin β1 and Arg interact both physically and functionally to activate p190RhoGAP and attenuate RhoA activity in the mouse brain. Moreover, genetic manipulations that reduce integrin β1 signaling through Arg recapitulate the hippocampal phenotypes observed in both *arg* $^{-/-}$ and conditional *itgb1* knock-out mice. Together, these results link integrin β1 with an Arg–p190RhoGAP pathway that promotes synapse maintenance, regulates dendritic arbor size, supports proper hippocampal function, and reduces the effects of cocaine in mice.

Previous work has strongly suggested a role for integrin β1 in the development of dendritic arbors. Application of integrin inhibitory peptides or expression of dominant-negative chimeric integrin β1 can each block dendritic growth in developing retinal ganglion neurons (Lilienbaum et al., 1995), and plating cortical neurons on integrin substrates such as laminin promotes dendritic branching and extension (Moresco et al., 2005). In addi-

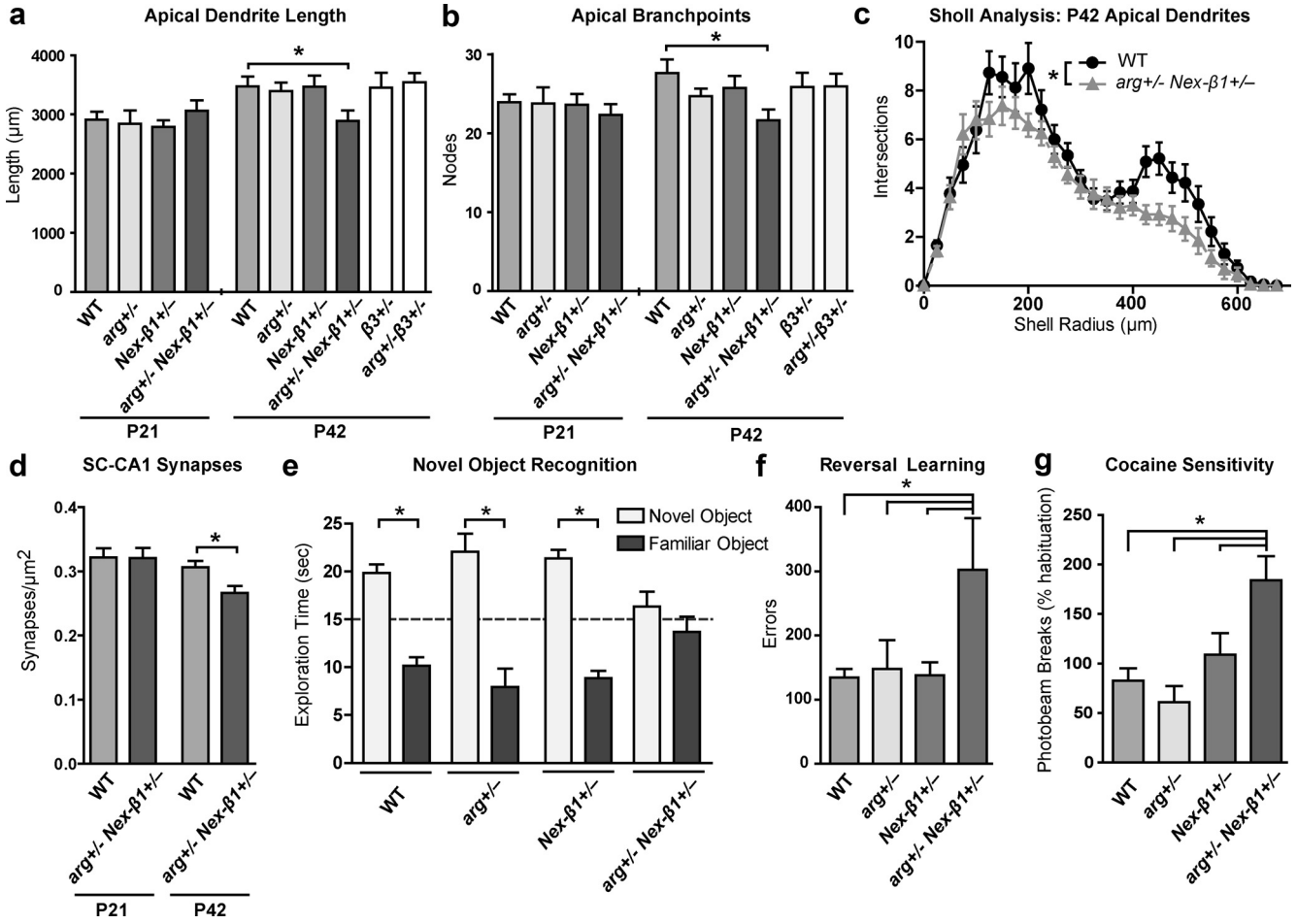

Figure 5. Arg and integrin β1 interact functionally to regulate synapse stability, dendritic arbor size, and behavior. ***a***, ***b***, Mean total dendrite length (***a***) and branch point number (***b***) of apical dendritic arbors of CA1 hippocampal neurons in WT and mutant mice at P21 and P42. *arg* $^{+/-}$*Nex-β1* $^{+/-}$ neurons were significantly smaller and had significantly fewer branch points than WT neurons at P42. One-way ANOVA and *post hoc* comparisons revealed no significant difference between genotypes at P21, but a significant effect of genotype at P42: length ($F_{(6,148)} = 3.105$; $p < 0.001$), branch point number ($F_{(6,146)} = 3.015$; $p < 0.001$). Student's *post hoc t* test for P42 *arg* $^{+/-}$*Nex-β1* $^{+/-}$ length, $p = 0.02$; branch point, $p = 0.009$, $n =$ 21–24 neurons for each genotype and age. ***c***, Sholl analysis of P42 dendrites from the same reconstructions revealed an overall reduction in *arg* $^{+/-}$*Nex-β1* $^{+/-}$ neurons. Main effect of genotype ($F_{(1,27)} = 5.858$; $p = 0.02$). ***d***, Mean SC–CA1 synapse density in WT and *arg* $^{+/-}$*Nex-β1* $^{+/-}$ mice at P21 and P42. Synapse density was reduced in *arg* $^{+/-}$*Nex-β1* $^{+/-}$ mice versus WT and P42, but not at P21. Student's *t* test, $p = 0.02$. P21, $n = 30$ sections, 2 mice for each group; P42 WT, $n = 94$ sections, 6 mice; P42 *arg* $^{+/-}$*Nex-β1* $^{+/-}$, $n = 57$ sections, 4 mice. ***e***, Quantification of time spent exploring a novel object in a hippocampus-dependent object recognition task at P42. WT, *arg* $^{+/-}$, and *Nex-β1* $^{+/-}$ mice spent significantly more time exploring the novel object, but *arg* $^{+/-}$*Nex-β1* $^{+/-}$ mice showed no significant preference between the novel and familiar object. *arg* $^{+/-}$ by *Nex-β1* $^{+/-}$ by object interaction ($F_{(1,68)} = 12.552$; $p < 0.001$). Student's *post hoc t* tests, $p < 0.05$. $n = 4$–13 mice per group. ***f***, Performance in a hippocampus-dependent spatial reversal learning task in adult mice. *arg* $^{+/-}$*Nex-β1* $^{+/-}$ committed significantly more errors (responses in the previously reinforced aperture) than WT, *arg* $^{+/-}$, or *Nex-β1* $^{+/-}$ mice. *arg* $^{+/-}$ by *Nex-β1* $^{+/-}$ interaction ($F_{(1,24)} = 5.1$; $p = 0.03$). Student's *post hoc t* tests, $p < 0.03$. $n = 5$–13 mice per group, >8 weeks of age. ***g***, Locomotor response to 10 mg/kg (intraperitoneal) of cocaine. Adult *arg* $^{+/-}$*Nex-β1* $^{+/-}$ displayed elevated cocaine sensitivity compared with WT, *arg* $^{+/-}$, and *Nex-β1* $^{+/-}$ mice. *arg* $^{+/-}$ by *Nex-β1* $^{+/-}$ interaction ($F_{(1,38)} = 5.1$; $p = 0.03$). Student's *post hoc t* tests, $p < 0.05$; $n = 7$–15 mice, >8 weeks of age. Values represent mean ± SEM. *$p < 0.05$ throughout.

tion, application of peptides that mimic the talin-binding domain of β1 or transfection of dominant-negative β1 tail constructs during development of chick retinal ganglion cells before synapse formation causes dendritic retraction (Marrs et al., 2006). However, we did not observe deficits in the initial formation of dendritic arbors; *itgb1* knock-out neurons developed normally through p21, but apical arbors were significantly reduced at P42. This result demonstrates a role for integrin β1 signaling in the late elaboration and maintenance, rather than initial formation, of hippocampal neuron structure.

Interestingly, the reduction in dendritic arbor size and complexity at P42 was limited to the apical arbor, similar to the phenotype observed in *arg* $^{-/-}$ neurons at this age (Sfakianos et al., 2007). This selectivity may be caused by the distribution of the relevant α integrin subunit or its upstream ligand, as some α integrins primarily localize to apical dendrites in the hippocampus (Bi et al., 2001). An alternative possibility is that consequences of Arg deficiency take place on different timescales in the distinct arbors *in vivo*. In support of this, although normal at P42, the basal dendritic arbors of hippocampal CA1 pyramidal neurons are significantly reduced at P120 in *arg* $^{-/-}$ mice (A. J. Koleske, unpublished data).

One obstacle in previous studies of integrin β1 functions in the forebrain has been the major defects in neuronal positioning associated with the loss of integrin β1 function in radial glia (Graus-Porta et al., 2001; Huang et al., 2006; Belvindrah et al., 2007). Here, we used a NEX-Cre line (Goebbels et al., 2006) to eliminate integrin β1 selectively in excitatory neurons. Previous work demonstrated that integrin β1 localizes to hippocampal synapses (Schuster et al., 2001) and that conditional genetic ablation of integrin β1 using CaMKII-Cre or emx1-Cre lines leads to reduced hippocampal synaptic efficacy and impaired synaptic

plasticity (Chan et al., 2006; Huang et al., 2006). Our results demonstrate that integrin β1 is largely dispensable for the early formation of synapses and dendrites through P21, but that loss of integrin β1 function leads to hippocampal synapse loss by P42. These results suggest that integrin β1 plays a role in maintenance of established synapses. Interestingly, no reduction in hippocampal synapse density was reported following inactivation of integrin β1 using CaMKII-Cre (Chan et al., 2006). As CaMKII-Cre is expressed significantly later than the NEX-Cre transgene used in these studies (Tsien et al., 1996), these observations raise the possibility that integrin β1 may play a critical role between E11.5 when NEX-Cre expression begins (Goebbels et al., 2006) and ~P25 when CaMKII-Cre is active (Tsien et al., 1996) and that inactivating integrin β1 after this period may not affect synapse maintenance and dendritic arborization. Although defects in age-dependent maturation of dendritic spine head size are observed in *arg*$^{-/-}$ mice (Sfakianos et al., 2007), our results demonstrate that knocking out *itgb1* does not affect spine morphogenesis, suggesting another upstream regulator may act through Arg to control spine shape refinement.

We report that conditional ablation of integrin β1 leads to deficits in a novel object recognition task. This behavioral defect is consistent with diminished hippocampal connectivity (Baker and Kim, 2002), and hippocampal lesions produce similar deficits (Broadbent et al., 2004). We also demonstrate that genetic ablation of integrin β1 from forebrain neurons leads to an increase in the hypermotor effects of cocaine. While studies have previously shown that cocaine changes the levels of integrin β1 signaling components (Wiggins et al., 2009; Chen et al., 2010), these results are the first to demonstrate that reducing integrin β1 expression can modulate the effects of cocaine. Although the anatomical studies in this report focus on the hippocampus, it is important to note that the effects of integrin β1 on cocaine sensitivity likely reflect contributions from other brain structures as well, since the NEX-Cre transgene knocks out expression in excitatory cortical neurons (Goebbels et al., 2006). In addition, *arg* knock-out also causes synapse and dendrite destabilization in the cortex (Koleske et al., 1998; Moresco et al., 2005; Gourley et al., 2009), and pharmacological inhibition of Arg selectively in prefrontal cortex leads to heightened cocaine sensitivity (Gourley et al., 2009). Therefore, defects in cortical structure and function also likely contribute to the *arg*$^{+/-}$*Nex-β1*$^{+/-}$ reversal learning and cocaine phenotypes (Gourley et al., 2010).

Previous studies in non-neuronal cells have demonstrated that adhesion to the integrin ligand fibronectin stimulates p190RhoGAP activity, which inactivates RhoA (Ren et al., 1999; Arthur et al., 2000; Bradley et al., 2006). Here, we provide the first evidence of a direct interaction between Arg and β1 and demonstrate that integrin β1 acts via Arg to regulate p190RhoGAP in neurons. Based on these results, along with previous studies on Arg–p190RhoGAP signaling in the nervous system (Hernández et al., 2004b; Sfakianos et al., 2007; Gourley et al., 2009), we propose a model wherein integrin β1-mediated adhesion stimulates Arg kinase activity, which leads to p120RasGAP:p190RhoGAP complex formation and RhoA inhibition (Fig. 6). Together, this cascade promotes neuronal stability, as excessive RhoA signaling leads to reductions in dendritic complexity and length (Threadgill et al., 1997; Ruchhoeft et al., 1999; Li et al., 2000; Nakayama et al., 2000; Sfakianos et al., 2007). In support of this model, we have previously demonstrated that reduced p190RhoGAP signaling leads to dendritic atrophy and that reducing RhoA activity rescues the dendrite loss seen in *arg*$^{-/-}$ mice (Sfakianos et al., 2007). Interestingly, reducing RhoA signaling does not prevent synapse loss in *arg*$^{-/-}$ mice (Sfakianos et al., 2007), suggesting that Arg may protect against synapse loss and dendritic retraction via distinct mechanisms.

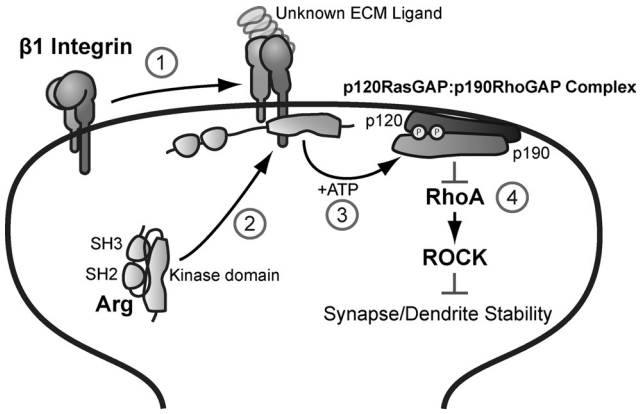

Figure 6. Model for integrin β1–Arg signaling in dendritic spines. (1) Integrin β1 is activated by binding to an unknown ligand. (2) The Arg kinase domain binds to the now exposed integrin β1 tail, stimulating Arg kinase activity by relieving autoinhibitory contacts between the SH3–SH2 domains and the kinase domain. (3) Arg phosphorylates p190RhoGAP, promoting its association with p120RasGAP at the membrane. (4) The p120RasGAP:p190RhoGAP complex inhibits RhoA, stabilizing synapses and dendrites.

What activates β1-containing integrins to promote synapse stabilization and increase dendrite arbor size? Extracellular space in the brain is filled with numerous ECM components that are integrin ligands (Sanes, 1989; Reichardt and Tomaselli, 1991), and acute application of peptides containing an arginine–glycine–aspartate (RGD) integrin β1 binding motif induce filopodia extensions and synaptic remodeling in cultured hippocampal neurons (Shi and Ethell, 2006). Of the integrin β1 ligands that are present at or near synapses and may regulate the β1–Arg–p190RhoGAP signaling cascade, laminin is a particularly promising candidate, as cultured *arg*$^{-/-}$ hippocampal neurons do not increase dendritic branching when plated on laminin compared with wild-type controls (Moresco et al., 2005). Importantly, changes in hippocampal laminin expression have been reported in human cocaine addicts (Mash et al., 2007), suggesting that integrin-mediated adhesion to laminin may affect vulnerability to cocaine addiction by regulating sensitivity. Alternatively, integrin β1–Arg signaling may be regulated by an unconventional integrin ligand such as Semaphorin7A (Pasterkamp et al., 2003; Moresco et al., 2005). Identification of the relevant upstream ligand and characterization of its developmental expression profile may also explain why the integrin β1–Arg signaling axis is essential for the late elaboration, but not initial formation of synapses and dendrites. Interestingly, the period of synapse and dendrite loss seen in both *arg*$^{-/-}$ and *Nex-β1*$^{-/-}$ mice coincides with late adolescence, a period marked by an increased vulnerability to addiction (Chambers et al., 2003; Gourley et al., 2009). However, it is currently unclear whether these reductions in neuronal connectivity are directly responsible for the behavioral abnormalities seen in *arg*$^{-/-}$ and *Nex-β1*$^{-/-}$ mice. Future studies should determine which ligands activate the β1–Arg–p190RhoGAP signaling cascade, and what effect they have on neuronal connectivity and function during this critical period in the corticostriatal and limbic regions known to be involved in addiction (Jentsch and Taylor, 1999).

References

Anton ES, Kreidberg JA, Rakic P (1999) Distinct functions of α3 and αV integrin receptors in neuronal migration and laminar organization of the cerebral cortex. Neuron 22:277–289.

Arias-Salgado EG, Lizano S, Sarkar S, Brugge JS, Ginsberg MH, Shattil SJ (2003) Src kinase activation by direct interaction with the integrin beta cytoplasmic domain. Proc Natl Acad Sci U S A 100:13298–13302.

Arthur WT, Petch LA, Burridge K (2000) Integrin engagement suppresses RhoA activity via a c-Src-dependent mechanism. Curr Biol 10:719–722.

Baker KB, Kim JJ (2002) Effects of stress and hippocampal NMDA receptor antagonism on recognition memory in rats. Learn Mem 9:58–65.

Belvindrah R, Graus-Porta D, Goebbels S, Nave KA, Müller U (2007) β1 integrins in radial glia but not in migrating neurons are essential for the formation of cell layers in the cerebral cortex. J Neurosci 27:13854–13865.

Benson DL, Schnapp LM, Shapiro L, Huntley GW (2000) Making memories stick: cell-adhesion molecules in synaptic plasticity. Trends Cell Biol 10:473–482.

Bi X, Lynch G, Zhou J, Gall CM (2001) Polarized distribution of alpha 5 integrin in dendrites of hippocampal and cortical neurons. J Comp Neurol 435:184–193.

Biederer T, Sara Y, Mozhayeva M, Atasoy D, Liu X, Kavalali ET, Südhof TC (2002) SynCAM, a synaptic adhesion molecule that drives synapse assembly. Science 297:1525–1531.

Blaess S, Graus-Porta D, Belvindrah R, Radakovits R, Pons S, Littlewood-Evans A, Senften M, Guo H, Li Y, Miner JH, Reichardt LF, Müller U (2004) β1-integrins are critical for cerebellar granule cell precursor proliferation. J Neurosci 24:3402–3412.

Bradley WD, Hernández SE, Settleman J, Koleske AJ (2006) Integrin signaling through Arg activates p190RhoGAP by promoting its binding to p120RasGAP and recruitment to the membrane. Mol Biol Cell 17:4827–4836.

Broadbent NJ, Squire LR, Clark RE (2004) Spatial memory, recognition memory, and the hippocampus. Proc Natl Acad Sci U S A 101:14515–14520.

Chambers RA, Taylor JR, Potenza MN (2003) Developmental neurocircuitry of motivation in adolescence: a critical period of addiction vulnerability. Am J Psychiatry 160:1041–1052.

Chan CS, Weeber EJ, Zong L, Fuchs E, Sweatt JD, Davis RL (2006) β1-integrins are required for hippocampal AMPA receptor-dependent synaptic transmission, synaptic plasticity, and working memory. J Neurosci 26:223–232.

Chavis P, Westbrook G (2001) Integrins mediate functional pre- and postsynaptic maturation at a hippocampal synapse. Nature 411:317–321.

Chen Q, Zhu X, Zhang Y, Wetsel WC, Lee TH, Zhang X (2010) Integrin-linked kinase is involved in cocaine sensitization by regulating PSD-95 and synapsin I expression and GluR1 Ser845 phosphorylation. J Mol Neurosci 40:284–294.

Dulabon L, Olson EC, Taglienti MG, Eisenhuth S, McGrath B, Walsh CA, Kreidberg JA, Anton ES (2000) Reelin binds alpha 3 beta 1 integrin and inhibits neuronal migration. Neuron 27:33–44.

Goebbels S, Bormuth I, Bode U, Hermanson O, Schwab MH, Nave KA (2006) Genetic targeting of principal neurons in neocortex and hippocampus of NEX-Cre mice. Genesis 44:611–621.

Gourley SL, Koleske AJ, Taylor JR (2009) Loss of dendrite stabilization by the Abl-related gene (Arg) kinase regulates behavioral flexibility and sensitivity to cocaine. Proc Natl Acad Sci U S A 106:16859–16864.

Gourley SL, Lee AS, Howell JL, Pittenger C, Taylor JR (2010) Dissociable regulation of instrumental action within mouse prefrontal cortex. Eur J Neurosci 32:1726–1734.

Gourley SL, Taylor JR, Koleske AJ (2011) Cell adhesion signaling pathways: first responders to cocaine exposure? Commun Integr Biol 4:30–33.

Graus-Porta D, Blaess S, Senften M, Littlewood-Evans A, Damsky C, Huang Z, Orban P, Klein R, Schittny JC, Müller U (2001) Beta1-class integrins regulate the development of laminae and folia in the cerebral and cerebellar cortex. Neuron 31:367–379.

Harburger DS, Calderwood DA (2009) Integrin signalling at a glance. J Cell Sci 122:159–163.

Harris KM, Stevens JK (1989) Dendritic spines of CA 1 pyramidal cells in the rat hippocampus: serial electron microscopy with reference to their biophysical characteristics. J Neurosci 9:2982–2997.

Hernández SE, Krishnaswami M, Miller AL, Koleske AJ (2004a) How do Abl family kinases regulate cell shape and movement? Trends Cell Biol 14:36–44.

Hernández SE, Settleman J, Koleske AJ (2004b) Adhesion-dependent regulation of p190RhoGAP in the developing brain by the Abl-related gene tyrosine kinase. Curr Biol 14:691–696.

Huang Z, Shimazu K, Woo NH, Zang K, Müller U, Lu B, Reichardt LF (2006) Distinct roles of the β1-class integrins at the developing and the mature hippocampal excitatory synapse. J Neurosci 26:11208–11219.

Jentsch JD, Taylor JR (1999) Impulsivity resulting from frontostriatal dysfunction in drug abuse: implications for the control of behavior by reward-related stimuli. Psychopharmacology 146:373–390.

Jones DH, Matus AI (1974) Isolation of synaptic plasma membrane from brain by combined flotation-sedimentation density gradient centrifugation. Biochim Biophys Acta 356:276–287.

Koleske AJ, Gifford AM, Scott ML, Nee M, Bronson RT, Miczek KA, Baltimore D (1998) Essential roles for the Abl and Arg tyrosine kinases in neurulation. Neuron 21:1259–1272.

Lapetina S, Mader CC, Machida K, Mayer BJ, Koleske AJ (2009) Arg interacts with cortactin to promote adhesion-dependent cell edge protrusion. J Cell Biol 185:503–519.

Leone DP, Relvas JB, Campos LS, Hemmi S, Brakebusch C, Fässler R, Ffrench-Constant C, Suter U (2005) Regulation of neural progenitor proliferation and survival by beta1 integrins. J Cell Sci 118:2589–2599.

Li Z, Van Aelst L, Cline HT (2000) Rho GTPases regulate distinct aspects of dendritic arbor growth in *Xenopus* central neurons in vivo. Nat Neurosci 3:217–225.

Lilienbaum A, Reszka AA, Horwitz AF, Holt CE (1995) Chimeric integrins expressed in retinal ganglion cells impair process outgrowth in vivo. Mol Cell Neurosci 6:139–152.

Marrs GS, Honda T, Fuller L, Thangavel R, Balsamo J, Lilien J, Dailey ME, Arregui C (2006) Dendritic arbors of developing retinal ganglion cells are stabilized by beta 1-integrins. Mol Cell Neurosci 32:230–241.

Mash DC, ffrench-Mullen J, Adi N, Qin Y, Buck A, Pablo J (2007) Gene expression in human hippocampus from cocaine abusers identifies genes which regulate extracellular matrix remodeling. PLoS One 2:e1187.

Moresco EM, Scheetz AJ, Bornmann WG, Koleske AJ, Fitzsimonds RM (2003) Abl family nonreceptor tyrosine kinases modulate short-term synaptic plasticity. J Neurophysiol 89:1678–1687.

Moresco EM, Donaldson S, Williamson A, Koleske AJ (2005) Integrin-mediated dendrite branch maintenance requires Abelson (Abl) family kinases. J Neurosci 25:6105–6118.

Nakayama AY, Harms MB, Luo L (2000) Small GTPases Rac and Rho in the maintenance of dendritic spines and branches in hippocampal pyramidal neurons. J Neurosci 20:5329–5338.

Parsons JT (1996) Integrin-mediated signalling: regulation by protein tyrosine kinases and small GTP-binding proteins. Curr Opin Cell Biol 8:146–152.

Pasterkamp RJ, Peschon JJ, Spriggs MK, Kolodkin AL (2003) Semaphorin 7A promotes axon outgrowth through integrins and MAPKs. Nature 424:398–405.

Peacock JG, Miller AL, Bradley WD, Rodriguez OC, Webb DJ, Koleske AJ (2007) The Abl-related gene tyrosine kinase acts through p190RhoGAP to inhibit actomyosin contractility and regulate focal adhesion dynamics upon adhesion to fibronectin. Mol Biol Cell 18:3860–3872.

Pinkstaff JK, Detterich J, Lynch G, Gall C (1999) Integrin subunit gene expression is regionally differentiated in adult brain. J Neurosci 19:1541–1556.

Reichardt LF, Tomaselli KJ (1991) Extracellular matrix molecules and their receptors: functions in neural development. Annu Rev Neurosci 14:531–570.

Ren XD, Kiosses WB, Schwartz MA (1999) Regulation of the small GTP-binding protein Rho by cell adhesion and the cytoskeleton. EMBO J 18:578–585.

Ruchhoeft ML, Ohnuma S, McNeill L, Holt CE, Harris WA (1999) The neuronal architecture of *Xenopus* retinal ganglion cells is sculpted by rho-family GTPases *in vivo*. J Neurosci 19:8454–8463.

Sanes JR (1989) Extracellular matrix molecules that influence neural development. Annu Rev Neurosci 12:491–516.

Schikorski T, Stevens CF (1997) Quantitative ultrastructural analysis of hippocampal excitatory synapses. J Neurosci 17:5858–5867.

Schlomann U, Schwamborn JC, Müller M, Fässler R, Püschel AW (2009) The stimulation of dendrite growth by Sema3A requires integrin engagement and focal adhesion kinase. J Cell Sci 122:2034–2042.

Schmid RS, Shelton S, Stanco A, Yokota Y, Kreidberg JA, Anton ES (2004) alpha3beta1 integrin modulates neuronal migration and placement during early stages of cerebral cortical development. Development 131: 6023–6031.

Schuster T, Krug M, Stalder M, Hackel N, Gerardy-Schahn R, Schachner M (2001) Immunoelectron microscopic localization of the neural recognition molecules L1, NCAM, and its isoform NCAM180, the NCAM-associated polysialic acid, beta1 integrin and the extracellular matrix molecule tenascin-R in synapses of the adult rat hippocampus. J Neurobiol 49:142–158.

Sfakianos MK, Eisman A, Gourley SL, Bradley WD, Scheetz AJ, Settleman J, Taylor JR, Greer CA, Williamson A, Koleske AJ (2007) Inhibition of Rho via Arg and p190RhoGAP in the postnatal mouse hippocampus regulates dendritic spine maturation, synapse and dendrite stability, and behavior. J Neurosci 27:10982–10992.

Shi Y, Ethell IM (2006) Integrins control dendritic spine plasticity in hippocampal neurons through NMDA receptor and Ca^{2+}/calmodulin-dependent protein kinase II-mediated actin reorganization. J Neurosci 26:1813–1822.

Sholl DA (1953) Dendritic organization in the neurons of the visual and motor cortices of the cat. J Anat 87:387–406.

Threadgill R, Bobb K, Ghosh A (1997) Regulation of dendritic growth and remodeling by Rho, Rac, and Cdc42. Neuron 19:625–634.

Tsien JZ, Chen DF, Gerber D, Tom C, Mercer EH, Anderson DJ, Mayford M, Kandel ER, Tonegawa S (1996) Subregion- and cell type-restricted gene knockout in mouse brain. Cell 87:1317–1326.

Van Aelst L, Cline HT (2004) Rho GTPases and activity-dependent dendrite development. Curr Opin Neurobiol 14:297–304.

Webb DJ, Zhang H, Majumdar D, Horwitz AF (2007) alpha 5 integrin signaling regulates the formation of spines and synapses in hippocampal neurons. J Biol Chem 282:6929–6935.

Wiggins AT, Pacchioni AM, Kalivas PW (2009) Integrin expression is altered after acute and chronic cocaine. Neurosci Lett 450:321–323.